applied sciences

MDPI

Article

Improved Adaptive NDI Flight Control Law Design Based on Real-Time Aerodynamic Identification in Frequency Domain

Dapeng Zhou [1,2], Zeyu Jin [3,*] and Guoqiang Wu [3]

[1] School of Aeronautic Science and Engineering, Beihang University, Beijing 100191, China; 18624064969@buaa.edu.cn
[2] Shenyang Aircraft Design and Research Institute, Shenyang 110034, China
[3] School of Aeronautics and Astronautics, Dalian University of Technology, Dalian 116024, China; gqwu@dlut.edu.cn
* Correspondence: 879301505@mail.dlut.edu.cn

Abstract: The traditional aircraft controller design is usually based on the off-line aerodynamic model. Due to the deviation of the off-line aerodynamic model, the flight quality is difficult to meet the requirements when the aircraft is flying in the real atmosphere. To solve this problem, this paper proposes a frequency domain identification-based improved adaptive nonlinear dynamic inversion (NDI) control method (FDI-ANDI). In this paper, an online recursive aerodynamic parameter identification method in the frequency domain is first designed, and then an adaptive dynamic inversion control method based on the online aerodynamic parameter identification results is established. Finally, aiming at the problem of the slow response speed of the NDI controller, an improved adaptive dynamic inversion control law is designed by using the method of series lead correction. Compared with the traditional control method, the adaptive dynamic inversion method based on online aerodynamic identification has stronger robustness and a faster response speed in the face of model uncertainty. The final simulation analysis shows that the method has a better control effect than the traditional control method.

Keywords: frequency domain; recursive least square; real-time aerodynamic identification; adaptive control; NDI control

check for updates

Citation: Zhou, D.; Jin, Z.; Wu, G. Improved Adaptive NDI Flight Control Law Design Based on Real-Time Aerodynamic Identification in Frequency Domain. *Appl. Sci.* **2023**, *13*, 6951. https://doi.org/10.3390/app13126951

Academic Editor: Shubo Wang

Received: 4 May 2023
Revised: 25 May 2023
Accepted: 29 May 2023
Published: 8 June 2023

Copyright: © 2023 by the authors. Licensee MDPI, Basel, Switzerland. This article is an open access article distributed under the terms and conditions of the Creative Commons Attribution (CC BY) license (https://creativecommons.org/licenses/by/4.0/).

1. Introduction

In the past few decades, the Unmanned Aerial Vehicle (UAV) has been greatly popularized in civil fields such as logistics and geological exploration [1,2]. Most of the control systems for UAVs are traditional controllers, such as PID controllers. However, due to the nonlinear characteristics of the real aircraft aerodynamic model, the control performance of the traditional methods cannot fully meet the expectations and their robustness behaves badly, which also brings secondary problems such as the long control system designing process. In order to overcome this problem, in recent years, a large number of studies have focused on the design of nonlinear control systems, such as adaptive control [3,4], intelligent control [5,6], and so on. Representative among these studies is the Learn-to-Fly project conducted by NASA's Langley Research Center [7,8].

Accurate acquisition of real-time dynamic information for aircrafts is the premise of nonlinear adaptive control adjustment. Aerodynamic identification can play a role in the whole life cycle of an aircraft. There are many different application scenarios, including aircraft offline aerodynamic model correction, aircraft adaptive controller design, and post-damage control reconstruction, etc. In some application scenarios, the aerodynamic identification must be carried out online, and the flight data collected by the sensor are obtained step by step, and finally, the accurate identification results are obtained. The method of aircraft dynamics identification includes two categories: time domain identification method and frequency domain identification method. The regression method represented

by the least square method is a kind of commonly used basic method, more methods have been created based on the least square method.

Ref. [9] combined the general least square method with the support vector machine (SVM) to achieve the predicted stable hysteresis loop. Ref. [10] introduced a method of Smoothed Partitioning with Localized Trees in Real Time (SPLITR), which uses a local model network for automatic real-time global aerodynamic modeling. In addition, the commonly used identification methods include maximum likelihood method [11,12], Kalman filter method [13,14] and so on.

As for the frequency domain, ref. [15] proposed a method to estimate the parameters of the linear model in real time by using the equation error of the recursive Fourier transform in the frequency domain. Ref. [16] established an equation error method in the frequency domain to estimate the dimensionless stability and control derivative in real time and had data forgetting, fusion prior information, and optimization excitation added. Ref. [17] introduced orthogonal optimized multi-sine inputs to excite aircraft dynamic response.

Intelligent methods are also gradually being used in aerodynamic identification. Ref. [18] used an adaptive neuro-fuzzy inference system extended by the Delta method (ANFIS-Delta) based on a feedforward neural network to estimate aerodynamic parameters to enhance the principle of an adaptive neuro-fuzzy inference system (ANFIS) in the Delta method. Ref. [19] applied a neural network to model the dynamic process of a canard-wing aircraft. In recent years, there have been many attempts to apply neural networks to aerodynamic identification [20–23].

In terms of nonlinear adaptive control methods, there are many different technical routes. For example, the series control system combined with a neural network or fuzzy controller and PID controller realizes online adjustment of control gain based on control error or other observations. Nonlinear dynamic inversion (NDI) control is also an adaptive control method which has strong adaptability and versatility. NDI control can better cope with the complicated decoupling work among different loops of nonlinear objects and does not need to repeatedly adjust the gain of each loop; it also has a great number of applications in aircraft nonlinear control in the long course of development. NDI control produces many different forms by adjusting the controller structure or combining with other controllers.

The NDI control based on L1 control is a representative direction. Ref. [24] proposed a new adaptive NDI control method based on L1 adaptive structure, called L1 Adaptive Nonlinear Dynamic Inversion (L1-ANDI), which can overcome the influence of interference and model uncertainty while ensuring the required dynamic performance. Ref. [25] also tried to introduce an L1 adaptive structure into NDI control to realize an adaptive DNI control method of an L1 adaptive structure with excellent dynamic performance and strong robustness. Combining it with a sliding mode control is another idea. Ref. [26] proposed a fault-tolerant control method based on an adaptive sliding mode, which can reduce the influence of time delay and sensor intermittent fault on the system and improve the stability of the inner loop controller. Ref. [27] combined baseline NDI control with advanced robust adaptive integral sliding mode (ISM) control to achieve acceptable flight quality at a high angle of attack under the influence of unknown disturbances and aerodynamic uncertainties.

Adaptive NDI control is widely used in damage reconstruction. Ref. [28] proposed a reconfigurable nonlinear dynamic inversion (RNDI) controller, which combines a nonlinear disturbance observer (NDO) and improved NDI control for attitude control of structurally damaged aircraft. Adaptive NDI control is also used in variable structure aircraft. In Ref. [29], an NDI flight controller is designed for the flight control of the swept wing morphing aircraft. Additional feedback is added to the nonlinear cancellation channel to improve the control law, which eliminates the influence of interference force, interference torque, and nonlinear cancellation error to a certain extent. NDI control is also used in the controller design of small UAVs [30].

In the engineering field, the traditional control method is often used. In past research, many results focused on the improvement of control effects through adaptive control methods. Most of these results remain in the theoretical research stage, and the engineering application value is not high.

This paper innovatively combines the frequency domain recursive aerodynamic parameter identification method with the NDI control method commonly used in the engineering field and realizes the adaptive NDI control method based on the identification results. On the one hand, this method introduces adaptive control to improve the control effect of the controller in the face of model uncertainty. On the other hand, the recursive identification method can ensure the real-time effect of identification and meet the needs of engineering applications.

Compared with previous studies, the method proposed in this paper takes into account the needs of engineering control methods while improving the flight control effect, and has a good improvement in control effect and practicability.

2. Article Structure Description and Aircraft Dynamics Modeling

Figure 1 shows the content structure of the article.

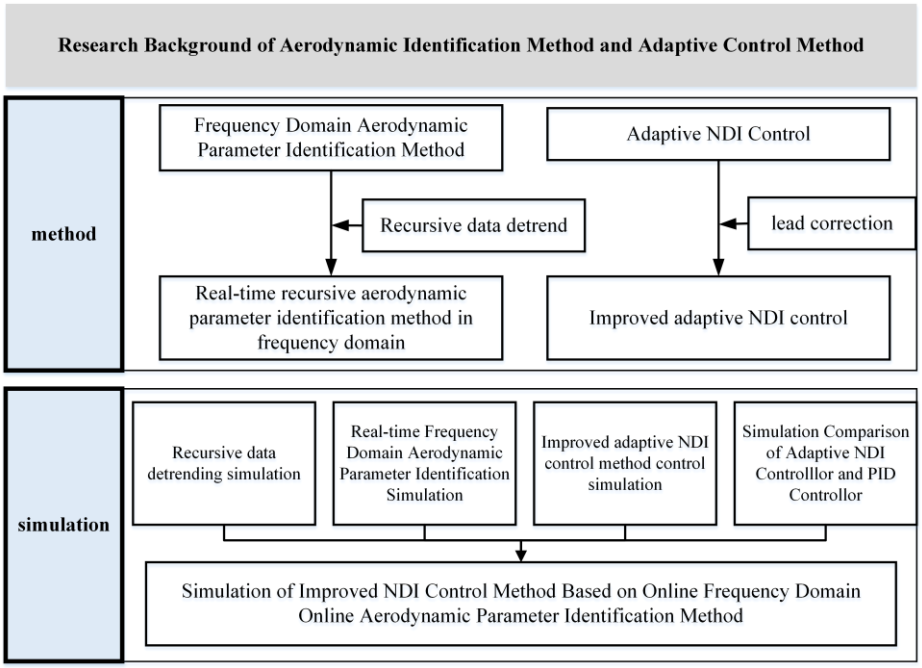


Figure 1. Structure of the article.

The dynamic equation of the aircraft centroid is [31]:

$$\begin{aligned} m(\dot{V}_x + qV_z - rV_y) &= F_x \\ m(\dot{V}_y + rV_x - pV_z) &= F_y \\ m(\dot{V}_z + pV_y - qV_x) &= F_z \end{aligned} \tag{1}$$

In the formula, m is the mass of the aircraft, $V = \begin{bmatrix} V_x & V_y & V_z \end{bmatrix}$ is the component of the aircraft speed in the airframe coordinate system, $\Omega = [p\ q\ r]$ is the component of the aircraft angular velocity in the airframe coordinate system, and $\begin{bmatrix} F_x & F_y & F_z \end{bmatrix}$ is the component of the combined external force of the aircraft in the airframe coordinate system. The upper point of the variable represents the derivative of the variable, and this setting also applies to the rest of this article.

Combined with the force analysis, the centroid dynamic equation of the aircraft is finally expressed as follows:

$$\begin{cases} m(\dot{V}_x + qV_z - rV_y) = -G\sin\theta + (-D\cos\alpha + L\sin\alpha) + T\cos\phi_{\mathrm{T}} \\ m(\dot{V}_y + rV_x - pV_z) = G\sin\phi\cos\theta + F_{\mathrm{Ay}} + F_{\mathrm{Ty}} \\ m(\dot{V}_z + pV_y - qV_x) = G\cos\phi\cos\theta + (-D\sin\alpha - L\cos\alpha) - T\sin\phi_{\mathrm{T}} \end{cases} \tag{2}$$

In the formula, G is the gravity of the aircraft, D is the aerodynamic drag, L is the aerodynamic lift, F_{Ay} is the aerodynamic lateral force, ϕ_T is the engine installation angle, and F_{Ty} is the lateral component of the engine thrust in the body coordinate system:

The aircraft inertia matrix I is:

$$I = \begin{bmatrix} I_{xx} & -I_{xy} & -I_{xz} \\ -I_{xy} & -I_{yy} & -I_{yz} \\ -I_{xz} & -I_{yz} & I_{zz} \end{bmatrix} \tag{3}$$

In the inertia matrix, $\begin{bmatrix} I_{xx} & I_{yy} & I_{zz} \end{bmatrix}$ respectively represent the moment of inertia of the aircraft around the three axes of the body coordinate system, and $\begin{bmatrix} I_{xy} & I_{xz} \dots & I_{yz} \end{bmatrix}$ denotes the product of inertia.

The angular momentum equation is:

$$H = \begin{bmatrix} H_x \\ H_y \\ H_z \end{bmatrix} = \begin{bmatrix} pI_{xx} - rI_{xz} \\ qI_{yy} \\ rI_{zz} - pI_{xz} \end{bmatrix} \tag{4}$$

In the formula, $\begin{bmatrix} H_x & H_y & H_z \end{bmatrix}$ are the components of angular momentum in the body coordinate system.

The motion of the aircraft around the center of mass can be expressed as:

$$\begin{bmatrix} \mathrm{d}H \\ \mathrm{d}t \end{bmatrix} = \begin{bmatrix} \dot{p}I_{xx} + qr(I_{zz} - I_{yy}) - (\dot{\omega}_z + pq)I_{xz} \\ \dot{q}I_{yy} - pr(I_{zz} - I_{xx}) + (p^2 - r^2)I_{xz} \\ \dot{r}I_{zz} + pq(I_{yy} - I_{xx}) + (q\dot{r} - \dot{p})I_{xz} \end{bmatrix} = \begin{bmatrix} L_A + L_T \\ M_A + M_T \\ N_A + N_T \end{bmatrix} \tag{5}$$

In the formula, $[L_a \ M_a \ N_a]$ are the components of the aerodynamic torque in the body coordinate system, and $[L_T \ M_T \ N_T]$ are the components of the torque generated by the thrust in the body coordinate system, respectively. Because gravity passes through the center of mass, it does not generate torque.

The torque equations are expressed as follows:

$$\begin{cases} \dot{p} = (c_1 r + c_2 p)q + c_3\overline{L} + c_4 N \\ \dot{q} = c_5 pr - c_6(p^2 - r^2)q + c_7 M \\ \dot{r} = (c_8 p + c_2 r)q + c_4\overline{L} + C_9 N \end{cases} \tag{6}$$

In this formula: $c_1 = \frac{(I_y - I_z)I_z - I_{xz}^2}{I_x I_z - I_{xz}^2}$, $c_2 = \frac{(I_x - I_y + I_z)I_{xz}}{I_x I_z - I_{xz}^2}$, $c_3 = \frac{I_z}{I_x I_z - I_{xz}^2}$, $c_4 = \frac{I_{xz}}{I_x I_z - I_{xz}^2}$, $c_5 = \frac{(I_z - I_x)}{I_y}$, $c_6 = \frac{I_{xz}}{I_y}$, $c_7 = \frac{1}{I_y}$, $c_8 = \frac{(I_x - I_y)I_x + I_{xz}^2}{I_x I_z - I_{xz}^2}$, $c_9 = \frac{I_x}{I_x I_z - I_{xz}^2}$.

Furthermore, it can be deduced that:

$$\begin{cases} \dot{\phi} = p + (r\cos\phi + q\sin\phi)\tan\theta \\ \dot{\theta} = q\cos\phi - r\sin\phi \\ \dot{\psi} = \frac{1}{\cos\theta}(r\cos\phi + q\sin\phi) \end{cases} \tag{7}$$

where ψ is the yaw angle.

3. Real-Time Frequency Domain Recursive Identification Method

The frequency domain recursive identification flow chart is as Figure 2.

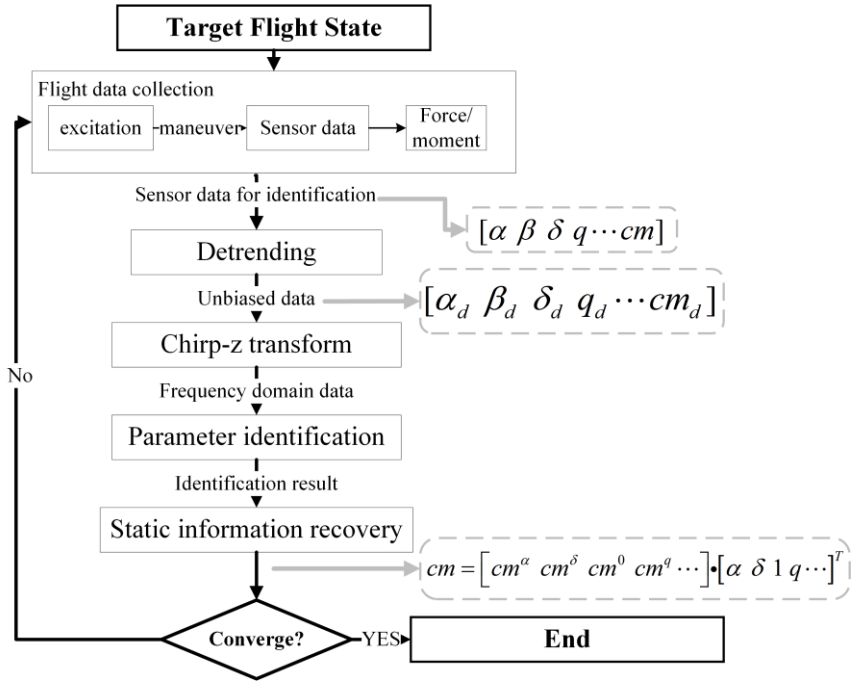


Figure 2. Frequency domain recursive identification process.

When performing aerodynamic identification, the aircraft needs to reach the predetermined flight state first, then the aircraft sensor obtains real-time flight data. The detrending program will detrend these data. These data are then converted from the time domain to the frequency domain using the Chirp-Z transform (CZT) method and are then recursively identified online. Finally, in the static information recovery part, the static information removed in the detrending part of these data will be restored.

There are several key steps in recursive identification in the frequency domain:

(1) Design an appropriate maneuvering mode to obtain flight data with valid information;
(2) Detrend the data, remove the information component, which is linear with time in the data, and retain the dynamic response information. In order to meet the needs of real-time control, it is necessary to use the recursive method to detrend;
(3) Chirp-z transform is used to transform the detrended flight data into the frequency domain.

3.1. Multi-Sinusoidal Rudder Excitation

When the aircraft is in a stable flight, the amount of information contained in the flight data is not sufficient. This low-information flight data cannot support accurate identification of the aerodynamic parameters of the aircraft. Therefore, an effective maneuver method must be adopted to improve the amount of information contained in the flight data to meet the needs of identification.

The method used in this paper is a multi-sinusoidal excitation signal [17]. It can be superimposed with the control instruction as the final control surface deflection instruction. The expression of this excitation signal is:

$$\mathrm{u}j = \sum_{\mathrm{k}\in\{1,2,\ldots,M\}} Ak \sin\left(\frac{2\pi kt}{T} + \phi\mathrm{k}\right) \tag{8}$$

Here, the disturbance input applied to the control surface j is set to u_j, which is the sum of the sine wave harmonics ϕ^k with a single-phase shift, where m is the total number of available harmonic correlation frequencies and T is the length of excitation time. A_k is the amplitude of the kth sine wave component and t is the time vector.

3.2. Recursive Detrending Method

In order to meet the real-time control of the aircraft, a real-time detrending method must be adopted. Here, a fourth-order Butterworth high-pass filter is used for detrending.

Here, there is a recursive method for filtering, which is a key point, because this method can be achieved in the real-time sensor data to trend, and ultimately, can obtain real-time identification results.

The expression of the filter can be written as a difference equation of the following rational transfer function:

$$\begin{aligned} a(1)y(n) = b(1)x(n) + b(2)x(n-1) + \ldots + b(n_b+1)x(n-n_b) \\ -a(2)y(n-1) - \ldots - a(n_a+1)y(n-n_a). \end{aligned} \tag{9}$$

In the formula, n_a is the order of the feedback filter, n_b is the order of the feedforward filter, $a\ (i)$ represents the denominator coefficient of the rational transfer function vector, $b\ (i)$ represents the molecular coefficient of the rational transfer function vector, $x\ (i)$ is the input data, $y\ (i)$ is the filtered data.

In order to achieve the purpose of recursive calculation, the following expressions can be written:

$$\begin{aligned} y(m) &= b(1)x(m) + w_1(m-1) \\ w_1(m) &= b(2)x(m) + w_2(m-1) - a(2)y(m) \\ \vdots &= \vdots \\ w_{n-2}(m) &= b(n-1)x(m) + w_{n-1}(m-1) - a(n-1)y(m) \\ w_{n-1}(m) &= b(n)x(m) - a(n)y(m). \end{aligned} \tag{10}$$

where $w\ (i)$ is the intermediate calculation variable, and the initial recursive value can be defined as constant 1.

3.3. Chirp-Z Transform

When the time domain data are converted to the frequency domain, the most commonly used method is the Discrete Fourier Transform (DFT) method, but the DFT method has some shortcomings for aircraft real time identification. Because it is usually necessary to pay attention to a small range of frequency bands, while DFT will introduce interference information, the Chirp-z Transform (CZT) method is used here.

The starting point z_0 of the CZT transform can be arbitrarily selected, so the narrowband high-resolution analysis of the input data can be performed from any frequency, and the frequency resolution can be adjusted as needed, so that any frequency band of interest can be accurately analyzed.

The results of the CZT transform are shown in Figure 3, where the red dots cover only one frequency range of interest.

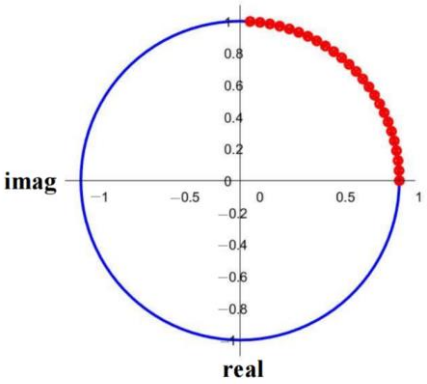


Figure 3. CZT transform effect illustration.

The steps of the CZT transform can be expressed as follows:

First, two L-point sequences $g\ (n)$ and $h(n)$ are constructed as follows:

$$g(n) = \begin{cases} A^{-n} W^{\frac{n^2}{2}} \times (n), 0 \le n \le N-1 \\ 0, \ \ N \le n \le L-1 \end{cases} \tag{11}$$

$$h(n) = \begin{cases} h(n) = W^{-\frac{n^2}{2}}, 0 \le n \le M-1 \\ h(n-L) = W^{-\frac{(n-L)^2}{2}}, M \le n \le L-1 \end{cases} \tag{12}$$

where L satisfies $L \ge N + M - 1$, and $L = 2^M$, M is an integer.

The Fourier transform $G\ (k)$ and $H\ (k)$ of $g\ (n)$ and $h\ (n)$ are calculated, respectively, and $Y\ (k) = G\ (k)\ H\ (k)$.

Then, the L-point inverse Fourier transform of $Y\ (k)$ is calculated by:

$$X(z_k) = W^{-\frac{n^2}{2}} y(n) \tag{13}$$

In order to achieve the effect of real-time identification, the conventional CZT transform process needs to combine the recursive finite Fourier transform mentioned in [17]:

$$X_i(\omega) = X_{i-1}(\omega) + x(i) e^{-j\omega i \Delta t} \tag{14}$$

$$e^{-j\omega i \Delta t} = e^{-j\omega \Delta t} e^{-j\omega (i-1) \Delta t} \tag{15}$$

3.4. Real-Time Aerodynamic Parameter Identification of Aircraft

The pitch moment coefficient of the aircraft can be simplified into the following form by linearization. Here, the moment is mainly concerned. It can be regarded as related to some flight state variables and satisfies an instantaneous linear relationship:

$$\begin{cases} C_l = C_{l_o} + C_{l_\beta}\beta + C_{l_\delta}\delta_{\text{ail}} + C_{l_p}\frac{\omega_x b}{2V} + C_{l_r}\frac{rb}{2V} \\ C_m = C_{m_o} + C_{m_\alpha}\alpha + C_{m_\delta}\delta_{ele} + C_{m_q}\frac{\omega_y \bar{c}}{2V} \\ C_n = C_{n_o} + C_{n_\beta}\beta + C_{n_\delta}\delta_{rdr} + C_{n_p}\frac{\omega_x b}{2V} + C_{n_r}\frac{vb}{2V} \end{cases} \tag{16}$$

In the formula, C_l, C_m, and C_n are pitching, yawing, and rolling moment coefficients. The lower right corner of the three variables represents the derivative of the moment coefficient of a variable to the lower right variable. The lower right corner is 0, representing the moment coefficient caused by the body configuration, b represents the wingspan length, and $\bar{c}$ represents the average aerodynamic chord length.

Sometimes, the modeling term on the right side of the equation also includes some high-order terms or coupling terms of different variables. Appropriate adjustments need to be made for different configurations of aircraft to accurately model, and a trade-off between the number of modeling variables and the amount of dynamic corresponding information is made, so as to achieve the purpose of accurately identifying and minimizing the amount of calculation.

Here, the pitch moment is taken as an example for analysis. The variable is defined as X, which is a vector composed of data obtained directly from the aircraft sensor. It contains the following contents:

$$X = [\alpha, \delta, \frac{\omega_y c}{2V}] \tag{17}$$

The detrending method introduced in the previous section can realize the recursive detrending of the data. The vector after the detrending is defined as X_d, the variable in the lower right corner "d" represents the detrended data of this variable, and X_d is expressed as follows:

$$X_d = [\alpha_d, \delta_d, \frac{\omega_y c}{2V}|_d] \tag{18}$$

The frequency domain sensor data $\widetilde{X}$ can be obtained by recursive Fourier transform, the superscript "$\sim$" represents the frequency domain data, and the expression of $\widetilde{X}$ is as follows:

$$\widetilde{X}_d = \begin{bmatrix} \alpha_d(1) & \delta_d(1) & \frac{\omega_y c}{2V}|_d(1) \\ \alpha_d(2) & \delta_d(2) & \frac{\omega_y c}{2V}|_d(2) \\ \cdots & \cdots & \cdots \\ \alpha_d(M) & \delta_d(M) & \frac{\omega_y c}{2V}|_d(M) \end{bmatrix} \tag{19}$$

In the frequency domain, the problem of a recursive solution can be expressed in the form of recursive least squares. The expression is as follows:

$$\widetilde{z}_d = \widetilde{X}_d\theta + \widetilde{e} \tag{20}$$

$$\widetilde{z}_d = \begin{bmatrix} \widetilde{C}_m(1) & \widetilde{C}_m(2) & \vdots & \widetilde{C}_m(M) \end{bmatrix}^T \tag{21}$$

$$\theta = \begin{bmatrix} C_{m_\alpha} & C_{m_{\delta_e}} & C_{m_{\frac{\omega_y c}{2V}}} \end{bmatrix}^T \tag{22}$$

The value of theta can be obtained by the following expression [16]:

$$\hat{\theta} = \left[\mathrm{Re}\left(\widetilde{X}^{\dagger}\widetilde{X}\right)\right]^{-1}\mathrm{Re}\left(\widetilde{X}^{+}\widetilde{z}\right) \tag{23}$$

In the formula, the variable with upper right corner "†" represents the complex conjugate transpose of this variable, and "Re" represents the real part of a complex number.

Eventually, we need to recover the static information C_{m0} filtered out of the trending process:

$$C_{m0} = C_m - \hat{\theta}X \tag{24}$$

4. Adaptive Disturbance Suppression Integrated Controller Design for UAV

4.1. NDI Controller Based on Real-Time Aerodynamic Parameter Identification

Figure 4 shows the structure of adaptive NDI control.

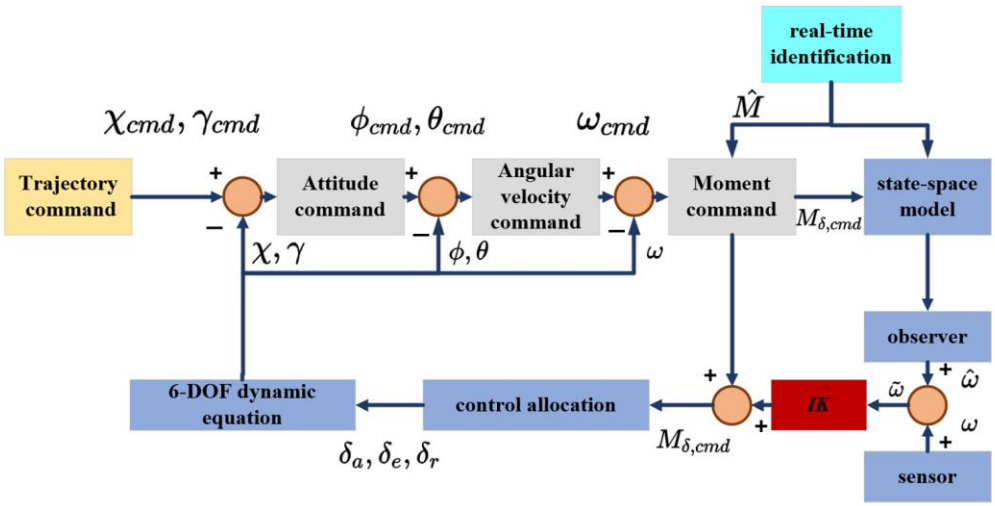


Figure 4. Adaptive NDI Controller Architecture.

Considering that the change of airflow angle α, β, γ is slower than that of angular velocity ω_x, ω_y, ω_z, the system is divided into a slow loop and fast loop. The inner slow loop dynamic inversion is to solve the next dynamic inversion command. According to the

instructions of roll angle ϕ, pitch angle θ, and angle of sideslip β, the instructions of ω_x, ω_y, and ω_z are solved.

$$\begin{cases} \omega_{xc} = K_\phi(\phi_c - \phi) - \tan(\theta)(\omega_z \sin(\phi) + \omega_y \cos(\phi)) \\ \omega_{yc} = -K_\beta(\beta_c - \beta) - \frac{g}{V}\sin(\phi) \\ \omega_{zc} = \frac{1}{\cos(\phi)}(K_\theta(\theta_c - \theta) + \omega_y \sin(\phi)) \end{cases} \tag{25}$$

The lower-right corner 'c' represents the instruction value of the variable, and this setting also takes effect in other parts of this article. K_ϕ, K_θ, K_β represents the gain of the controller.

Bringing the above control instructions back to the dynamic equation, we can obtain:

$$\begin{cases} \dot{\phi} = K_\phi(\phi_c - \phi) \\ \dot{\theta} = K_\theta(\theta_c - \theta) \\ \dot{\beta} = K_\beta(\beta_c - \beta) \end{cases} \tag{26}$$

According to the solution formula of first-order linear non-homogeneous differential equation, we can obtain:

$$\begin{cases} \phi = \phi_c + (\phi(0) - \phi_c)e^{-K_\phi t} \\ \theta = \theta_c + (\theta(0) - \theta_c)e^{-K_\theta t} \\ \beta = \beta_c + (\beta(0) - \beta_c)e^{-K_\beta t} \end{cases} \tag{27}$$

The time domain response function in the same form as the orbital angle can be obtained, and convergence can be achieved in a limited time.

By solving the inverse of the dynamic equation of the inner loop to track these angular rate commands, the required angular acceleration proportional to the angular rate error can be obtained by:

$$M_c = IK_\omega(\omega_c - \omega) - (\hat{M} - \omega \times I\omega) \tag{28}$$

In the formula, M represents moment, $\hat{M}$ is determined by the current identification model of the aircraft, and K_ω is the control gain.

Substituting the control torque command into $\dot{\omega}$ in the kinetic equation gives, in the formula, M as the torque value obtained by the sensor.

$$\dot{\omega} = K_q(\omega_c - \omega) + I^{-1}(M - \hat{M}) \tag{29}$$

Combined with the results of real-time identification in the frequency domain, the final control rudder deflection solution can be expressed as:

$$\delta_c = \frac{C_{m_c} - (C_{m_\alpha} \times \alpha + C_{m_{\frac{\omega c}{2V}}} \times \frac{\omega c}{2V} + C_{m_0})}{C_{m_\delta}} \tag{30}$$

4.2. Improved NDI Controller Design

Aiming at the problem of large error and strong hysteresis based on conventional dynamic inversion under an unsteady aerodynamic force, an improved adaptive NDI control method is introduced, improving the control effect in the presence of errors in aerodynamic identification results.

The leading link is added when solving the nominal angular rate in the slow loop [32]. The conventional slow loop angular rate solving law is as follows:

$$\omega_c = K_\theta(\theta_c - \theta) \tag{31}$$

After adding the lead link, the expression becomes:

$$\omega_{c_{imp}} = \frac{s/\omega_C + 1}{s/\omega_D + 1} \cdot K_\theta(\theta_c - \theta) = \frac{s/\omega_C + 1}{s/\omega_D + 1} \cdot q_c = \frac{K_C s + 1}{K_D s + 1} \cdot \omega_c \tag{32}$$

Written in the form of time domain:

$$K_D \cdot \dot{\omega}_{c_{imp}}(k) + \omega_{c_{imp}}(k) = K_C \cdot \dot{\omega}_c(k) + \omega_c(k) \tag{33}$$

where q_{Cimp} is the improved expected angular velocity. Using approximate difference instead of differential, the nominal angular rate after adding the leading link is obtained:

$$\omega_{c_{imp}}(k) = \frac{\left[\frac{K_D}{\tau}\omega_{c_{imp}}(k-1) - \frac{K_C}{\tau}\omega_c(k-1) + \left(\frac{K_C}{\tau}+1\right)\omega_c(k)\right]}{\left(\frac{K_D}{\tau}+1\right)} \tag{34}$$

5. Simulation Result and Discussion

This section shows the simulation results and analysis of the two main research contents.

Real-time flight data are obtained from flight simulation, and the real-time data are recursively detrended. Then, they are substituted into the frequency domain recursive identification program to determine the accuracy of the identification. In this process, it is necessary to evaluate the recursive effectiveness of online flight data, so as to set some necessary process settings, such as time delay, for the whole process simulation.

The second part compares the control effects between the conventional PID controller and the NDI controller, and then introduces the improved NDI controller with advanced correction to compare the control effects of the three and verify the robustness of the improved NDI controller. Finally, the whole process simulation including the real-time frequency domain identification and improved adaptive NDI control is given, which proves that the method designed in this paper can meet the requirements of real-time operation.

5.1. Real-Time Frequency Domain Identification Simulation

Applying an active excitation signal to the control surface can stimulate the dynamic characteristics of the aircraft, so that the flight data contain more information and improve the accuracy of identification. In this paper, only the longitudinal pitch force distance identification is concerned, so only the elevator is applied. The excitation expression is:

$$\mathrm{u} = 0.5 \times (\sin(\frac{4\pi t}{T} + 2.8274) + \sin(\frac{8\pi t}{T} + 2.1991) + \sin(\frac{12\pi t}{T}) + \sin(\frac{16\pi t}{T} + 1.8850)) \tag{35}$$

The image of each sine signal and the effect of their superposition are shown in Figure 5.

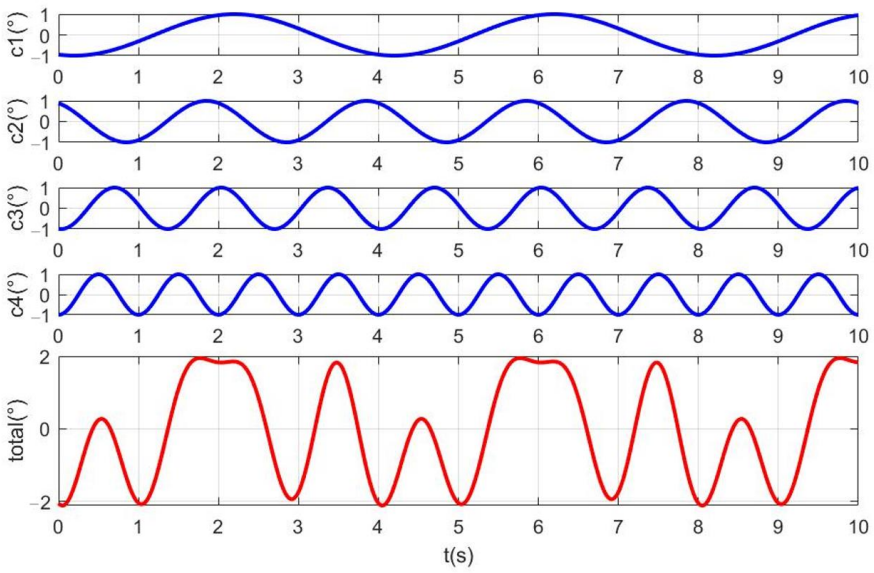


Figure 5. Actuator surface excitation component.

The flight state of the identification phase selected in this paper is shown in the Figure 6.

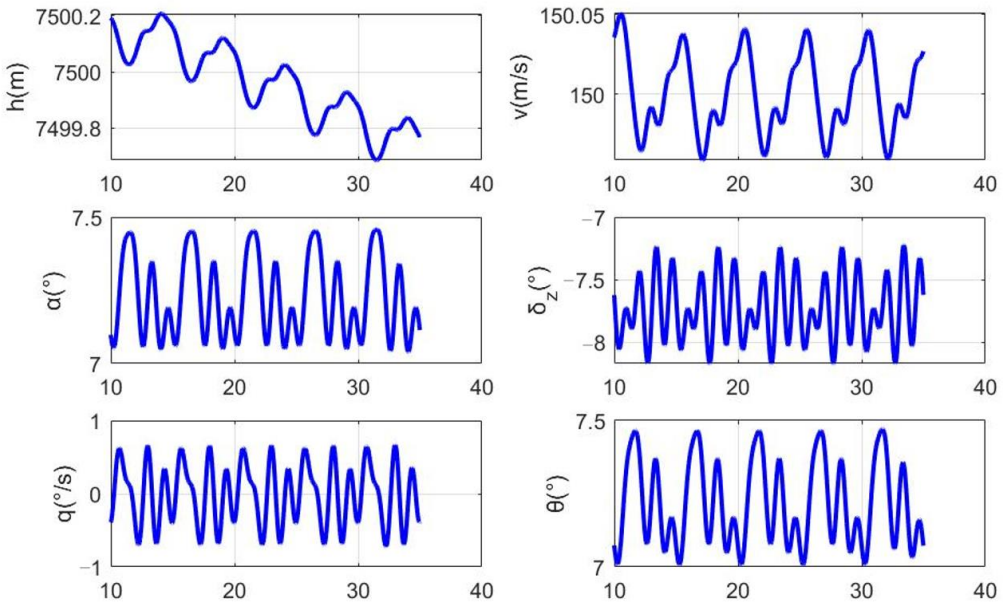


Figure 6. Flight state in real-time parameter identification phase.

Flight altitude is about 5000 m, speed is about 150 m/s, in the horizontal flight state dynamics identification.

A 4-order Butterworth high-pass filter is used, Table 1 shows the specific information of the filter.

Table 1. Filter configuration.

Description	Symbol
filter types	Butterworth
order	4
sampling frequency	100
cut-off frequency	0.1

In order to realize real-time identification, the flight data have to be detrended. The comparison of data before and after processing is shown in the figure below.

In Figure 7, the blue solid line represents the untreated original data. When the data has a constant component or a component that is linearly related to time, after being converted into the frequency domain, there will be a high-peak low-frequency component, which affects the identification accuracy. In the above figure, it can be clearly seen that the angle of attack and the elevator angle have obvious constant components, so these data must be processed. Relatively speaking, the other two have small deviations, but they also need to be processed.

The red solid line in the diagram is the result of real-time recursive detrending. In order to observe the detrending effectiveness more intuitively, after the simulation is completed, a more accurate batch detrending method is used offline for data processing, and all the results are displayed in a picture. It must be pointed out that this batch method does not meet the needs of real-time operation, because it requires simultaneous processing of all flight data. If all the previous data are processed in batches after each data acquisition, the effect of the similar inference method can be achieved. However, this will cause a very large amount of calculation and put forward high requirements for the hardware computing power of the aircraft. The results of offline batch processing are represented by blue dashed

lines. It can be clearly seen from the figure that it takes about 20 s to converge the nevus with the same accuracy as the batch processing method. This is because at the initial time, for the lack of flight data, the constant components contained in the flight data cannot be accurately identified.

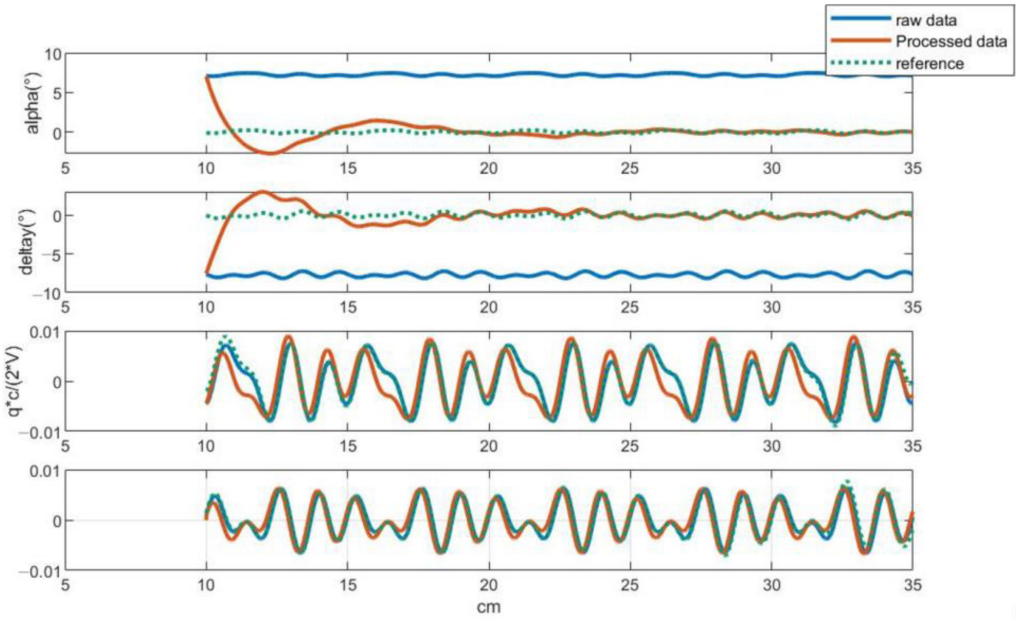


Figure 7. Comparison of Flight Data Before and After Detrending and Reference Standard Curve.

Through this experiment, a conclusion can be drawn that when using the recursive real-time detrending method, it is necessary to wait for a period of time after starting the detrending process to carry out the recursive aerodynamic identification. The specific waiting time length should be determined by flight data analysis. Here, the waiting time is 20 s.

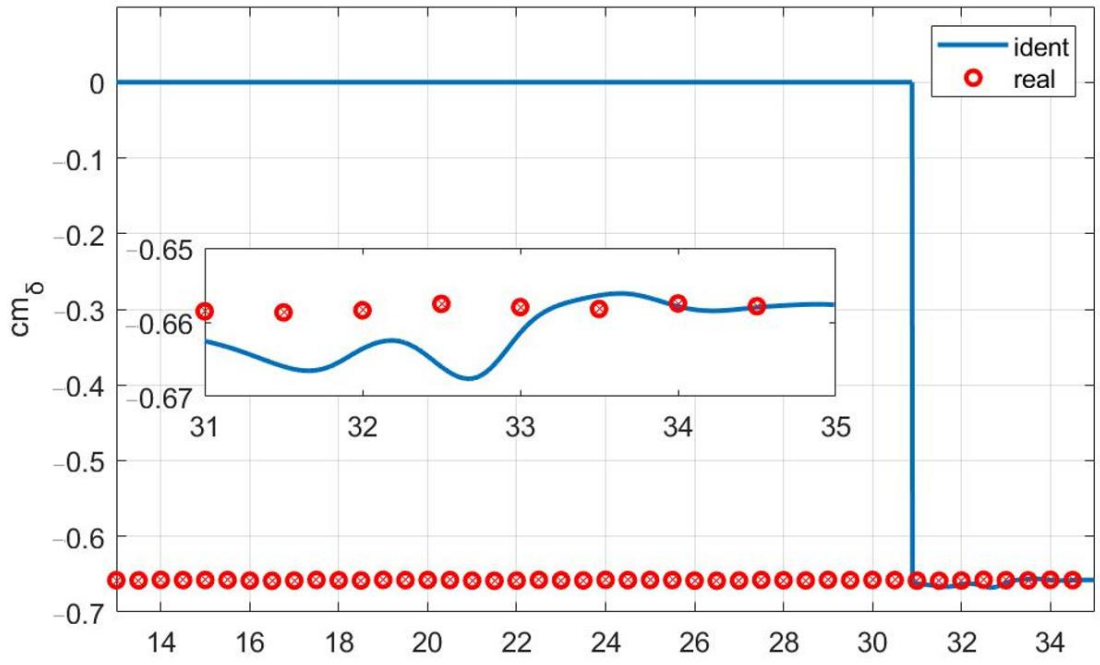
After the detrending, the frequency domain recursive identification can be performed. Figure 8 shows the identification results.

In the stage of waiting for the convergence of the real-time filter, the identification result is artificially set to 0. In order to ensure that the identification result fluctuates greatly at the beginning of the recursion, the first 90 samples are taken for one batch, and the result is used as the initial value for subsequent recursion.

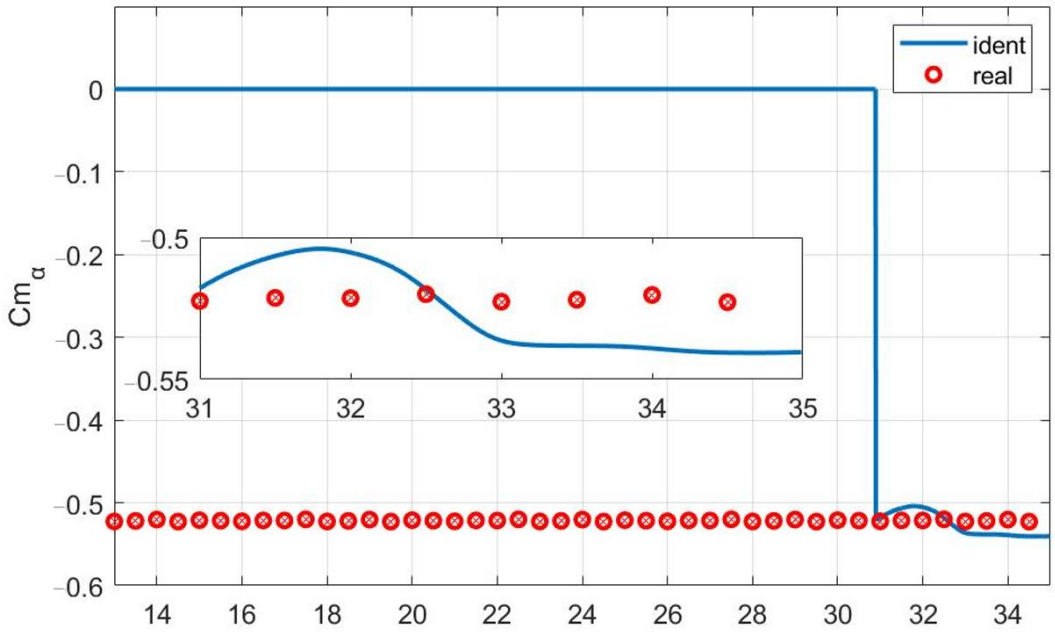
In the above diagram, it can be seen that the initial value error obtained after batch processing is very small, and the identification result is stable in the subsequent recursive process, which can show that the identification is rapid, the convergence is great, and the error is small. In order to explain the identification accuracy more clearly, after the recursion starts, a time interval with stable identification results is selected to average the relative error of parameter identification. Table 2 shows the aerodynamic coefficient identification results.

Table 2. Relative error of real-time aerodynamic parameter identification.

Description	Mean Relative Deviation (%)
$C_{m\alpha}$	−0.9084
$C_{m\delta}$	−0.4896



(**a**)



(**b**)

Figure 8. Real-time parameter identification results. subplot (**a**,**b**) are the derivatives of the pitch moment coefficient to the deflection angle and angle of attack of the elevator, respectively.

The error of the aerodynamic parameter identification results is within 1%, which meets the accuracy requirements of real-time control adjustment.

5.2. NDI Control Simulation Based on Real-Time Aerodynamic Parameter Identification

This section first uses the conventional NDI controller for simulation and compares the control effect between the NDI controller and the PID controller under the step pitch angle command.

After the recursive identification achieves convergence, The control switch will trigger the controller switching to NDI control mode, then use the PID controller and NDI controller to track the pitch angle step command, respectively. Since the accuracy of identification has been explored and explained in detail in the previous section, this section only shows the image of the instruction tracking part.

In this section, the initial state of the aircraft is given as follows, and the step instruction is 10°. Table 3 shows the simulation initial conditions.

Table 3. Simulation initial state.

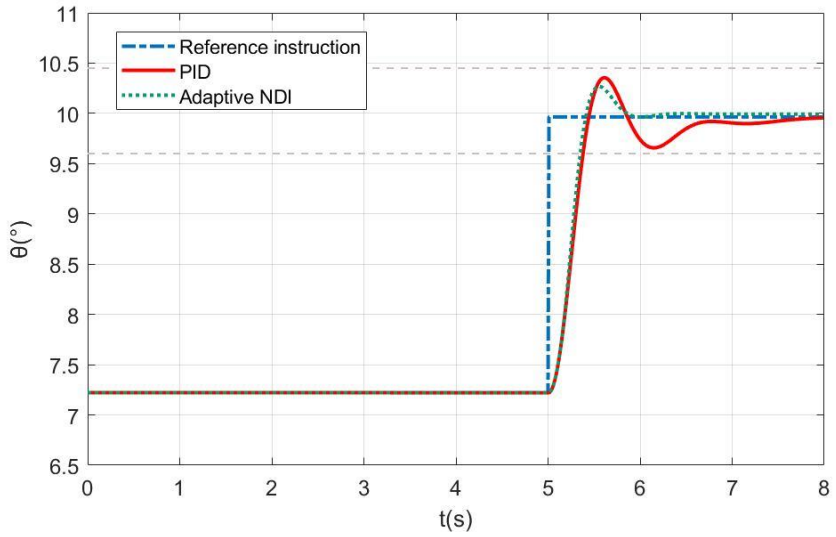
Description	Symbol	Value
pitching angle	θ	7.25°
angle of attack	α	7.25°
elevator	δ_{ele}	−7°
altitude	H	7500 m
speed	V	150 m/s

Figure 9 is the NDI controller and PID controller pitch angle control effect comparison.

In the simulation diagram, it can be clearly seen that compared with the PID controller, the NDI controller responses faster with a smaller overshoot. From the elevator deflection angle image and the pitch angular rate image, it can be seen that the NDI controller can simultaneously achieve a larger angle of the rudder deflection and faster adjustment response when controlling the aircraft to track the step pitch angle command, so as to achieve a better control effect. In order to compare the differences between the two numerically, three indicators of the rise time, peak time, and overshoot are selected to quantitatively compare the control effects of the two.

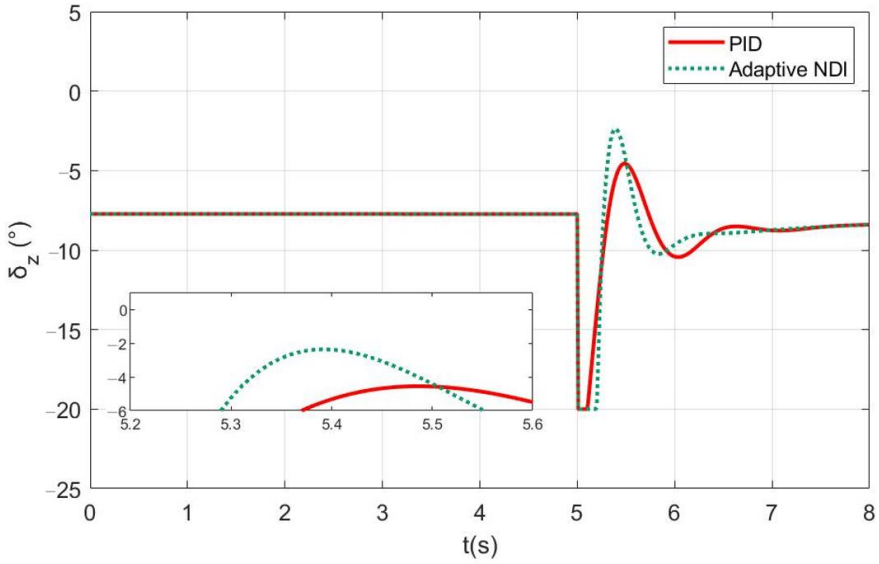
The definitions of the three indicators are:

(1) Overshoot: The ratio of the instantaneous maximum deviation (θ_{emax}) to the steady-state value (θ_∞), expressed in a percentage.
(2) Rise time: The time required for the response curve to rise from 10% of the steady-state value to 90% of the steady-state value.
(3) Peak time: Time it takes for a step response curve to exceed its steady-state value to reach its first peak.

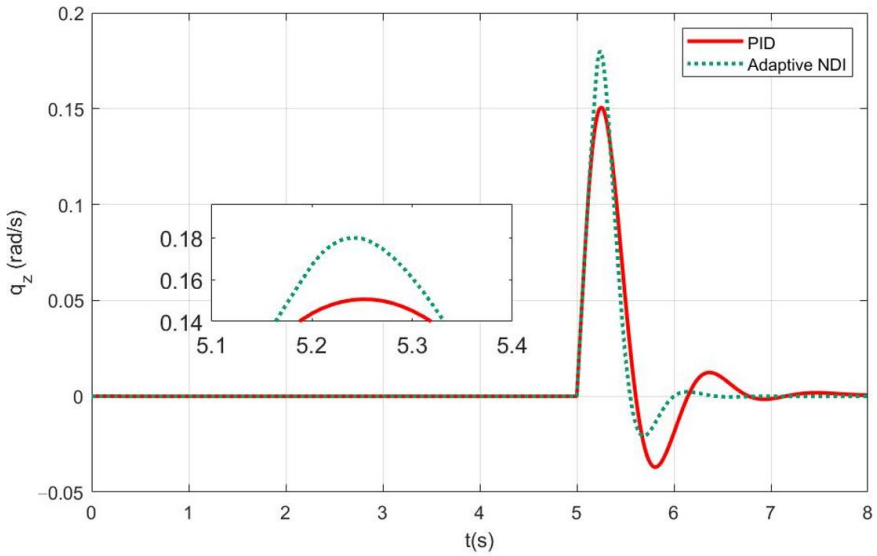


(**a**)

Figure 9. *Cont.*



(**b**)



(**c**)

Figure 9. Comparison of NDI and PID control effects. subplot (**a**–**c**) are pitch angle, elevator deflection angle and pitch angle velocity, respectively.

Table 4 shows the quantitative comparison of simulation results.

Table 4. Control effect index comparison (NDI vs. PID).

Description	PID Controller	NDI Controller
rise time(s)	0.39	0.36
peak time(s)	0.61	0.55
overshoot (%)	35.21	26.78

According to the three indicators defined here, the control effects of different controllers can be quantitatively compared. Combined with simulation images and numerical analysis, it can be seen that compared with the traditional PID controller, the adaptive NDI controller can make the aircraft converge to the target command faster, and the response

speed is faster, the overshoot is smaller, and the convergence speed is faster, indicating that the adaptive NDI controller has better control effect.

5.3. Simulation Verification of Improved Adaptive Control Method

Under the same conditions as Section 5.2, the simulation verification of the improved NDI control method is carried out. Similarly, in the simulation of this section, all links including recursive detrending, identification, and step pitch angle command are also used, and only the image of the step command tracking stage is displayed.

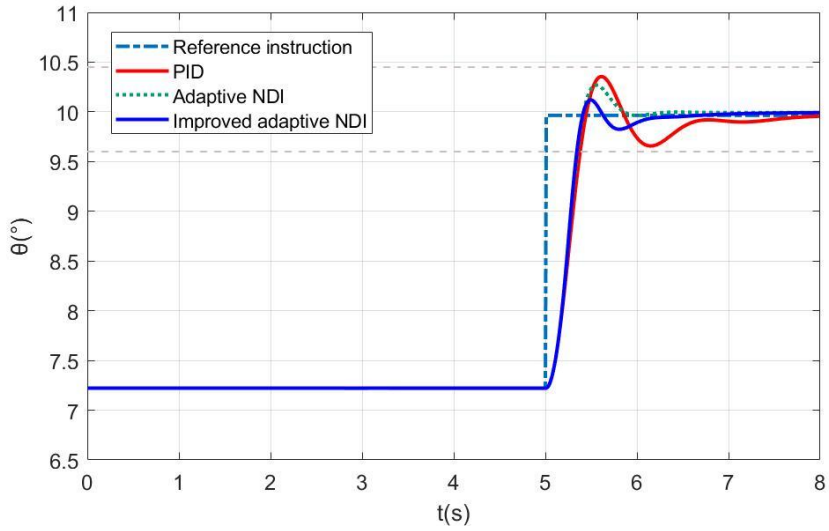
Figure 10 shows the step response tracking effect of the improved NDI control method, conventional NDI control, and PID control.

It can be seen from the simulation diagram that compared with the PID controller and the NDI controller, the improved NDI controller has a further improvement in response speed and overshoot. Similarly, it can be seen from the elevator deflection angle image and the pitch angle velocity image that the improved NDI controller has a better response effect of the elevator deflection angle. In order to compare the differences among the two numerically, three indicators of rise time, peak time, and overshoot are selected to quantitatively compare the control effects of the three. Table 5 shows the quantitative comparison of simulation results.

Table 5. Control effect index comparison (INDI vs. NDI vs. PID).

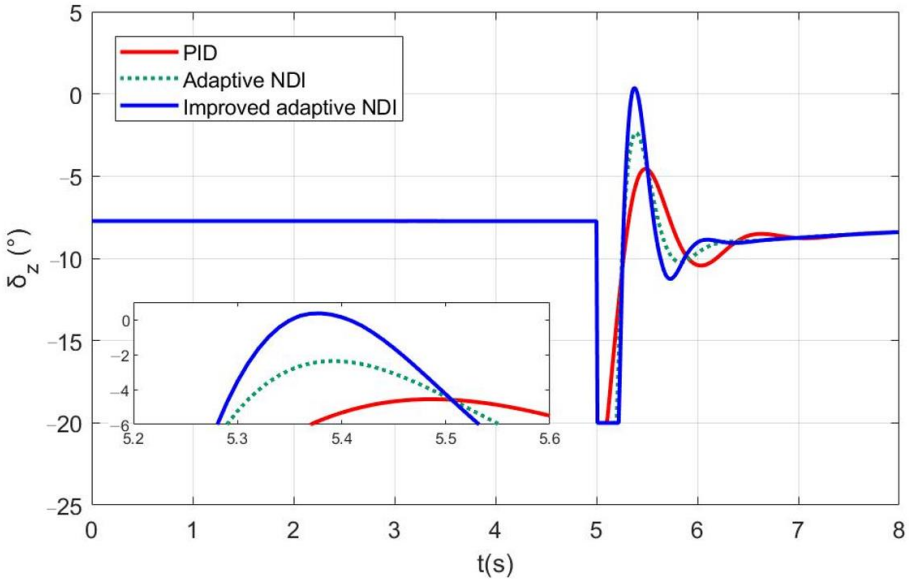
Description	PID	NDI	Improver NDI
rise time(s)	0.39	0.36	0.35
peak time(s)	0.61	0.55	0.49
overshoot (%)	35.21	26.78	11.97

Under the same simulation conditions, compared with the improved NDI, adaptive NDI and PID control methods, it can be seen that the improved NDI has faster response speed and convergence speed than the adaptive NDI, and the overshoot is smaller. It has the best control effect among the three, which shows the effectiveness of the series lead link.

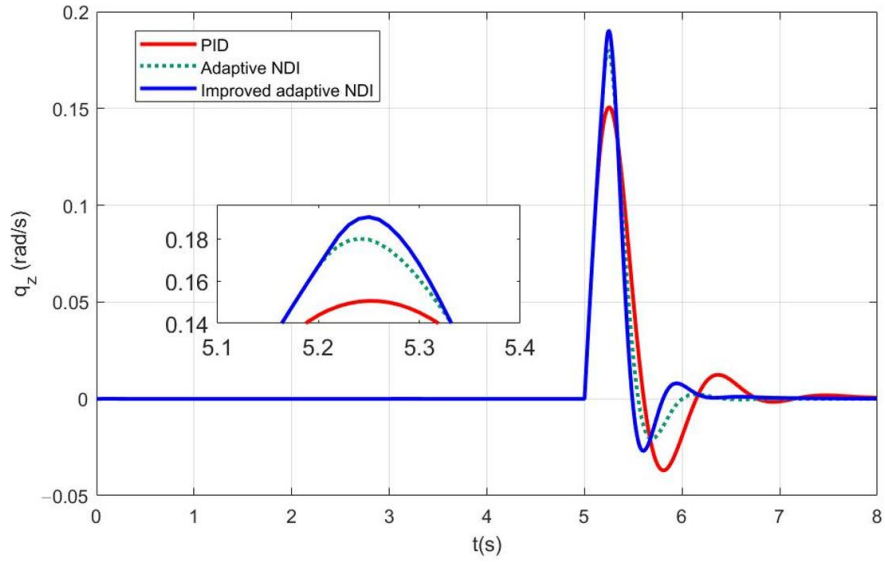


(**a**)

Figure 10. *Cont.*



(**b**)



(**c**)

Figure 10. INDI, NDI and PID control effect comparison. subplot (**a**–**c**) are pitch angle, elevator deflection angle and pitch angle velocity, respectively.

5.4. Whole Process Simulation of Improved NDI Control Based on Real-time Frequency Domain Identification

Since this paper focuses on a whole process method combining real-time aerodynamic identification and adaptive NDI control, the whole process simulation is carried out on the basis of the above verification of each part.

The simulation process of this section includes: real-time recursive detrend, real-time recursive parameter identification, step command tracking, free flight phase, as Figure 11 shows.

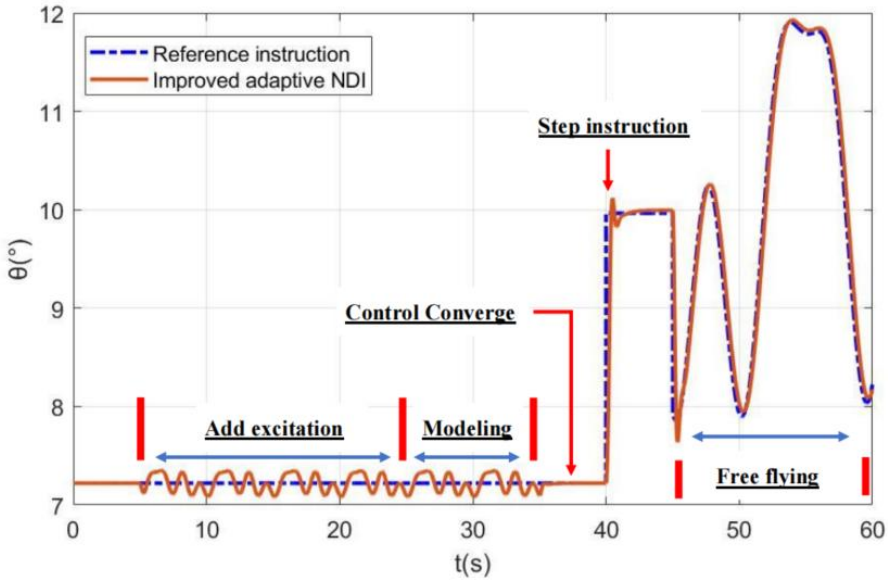


Figure 11. Whole Process Simulation of Improved NDI Control Based on Real-time Frequency Domain Identification.

In the whole flight phase, the flight attitude of the aircraft is stable, the command response is fast, and the attitude command with large variation can also be accurately tracked to meet the design requirements.

6. Conclusions

Aiming at the problem of poor robustness of traditional controllers under nonlinear conditions such as model uncertainty, this paper designs an improved adaptive NDI control method based on real-time aerodynamic parameter identification in the frequency domain. Firstly, the online frequency domain aerodynamic parameter identification method is introduced, including the setting of the excitation signal, recursive flight data detrending, CZT transform, and recursive identification steps. Then, the solution process of the adaptive NDI method based on real-time aerodynamic identification is introduced. Based on it, an improved NDI control method is introduced to improve the control response speed. In the final simulation part, the aerodynamic parameters are identified by the real-time identification method introduced in this paper. The identification error is within 1%, which meets the requirements of adaptive control. Then, the performance of the PID controller and adaptive NDI controller in aircraft attitude control is compared. Through quantitative comparative analysis, it is proved that the adaptive NDI controller is superior to the PID controller in terms of rising speed, response speed, and overshoot. By introducing an improved adaptive NDI controller for comparative simulation, it is concluded that the controller has better control effect, which shows the feasibility of the method introduced in this paper. The frequency domain online identification introduced in this paper can achieve accurate online identification, and on this basis, an improved adaptive NDI controller is used to achieve accurate attitude control. At the same time, because the method proposed in this paper can be recursively operated step by step, the calculation amount of online identification is reduced, which is of great significance in practical engineering application.

The innovation of the method proposed in this paper is mainly to combine frequency domain identification with the improved adaptive NDI control method, to design an adaptive control method that can be realized in engineering. It can use flight data to identify and optimize the control effect of the controller in real time.

This highly engineered method can be applied to the design of commercial aircraft to simplify the control system design process and save costs. At the same time, it can be applied to improve the flight controller using the conventional NDI control method to

improve its control effect. This improvement has a good application prospect in some application scenarios that require high flight control quality.

Author Contributions: Conceptualization, D.Z. and G.W.; methodology, D.Z. and G.W.; software, D.Z.; validation, D.Z. and Z.J.; formal analysis, D.Z., Z.J. and G.W.; investigation, D.Z. and Z.J.; resources, D.Z. and Z.J.; data curation, D.Z. and Z.J.; writing—original draft preparation, D.Z. and G.W.; writing—review and editing, D.Z., Z.J. and G.W.; visualization, D.Z. and Z.J.; supervision, D.Z. and G.W.; project administration, D.Z. and G.W.; funding acquisition, D.Z. All authors have read and agreed to the published version of the manuscript.

Funding: This research was funded by National Natural Science Foundation of China, grant number U2141229 and foundation under grant JCJQ, grant number 2019-JCJQ-DA-001-131.

Institutional Review Board Statement: Not applicable.

Informed Consent Statement: Not applicable.

Data Availability Statement: Not applicable.

Conflicts of Interest: The authors declare no conflict of interest.

Nomenclature

The following abbreviations are used in this manuscript.

Acronym	Full Name
NDI	Nonlinear Dynamic Inversion
FDI-ANDI	Frequency Domain Identification based Improved Adaptive NDI Control
UAV	Unmanned Aerial Vehicle
SVM	Support Vector Machine
SPLITR	Smoothed Partitioning with Localized Trees in Real Time
ANFIS	Adaptive Neuro-fuzzy Inference System
ANFIS-Delta	Adaptive Neuro-fuzzy Inference System Extended by Delta Method
L1-ANDI	L1 Adaptive Nonlinear Dynamic Inversion
ISM	Integral Sliding Mode
RNDI	Reconfigurable Nonlinear Dynamic Inversion
NDO	Nonlinear Disturbance Observer
CZT	Chirp-Z Transform
DFT	Discrete Fourier Transform

References

1. Hii, M.S.Y.; Courtney, P.; Royall, P.G. An Evaluation of the Delivery of Medicines Using Drones. *Drones* **2019**, *3*, 52. [CrossRef]
2. Natesan, S.; Armenakis, C.; Benari, G.; Lee, R. Use of UAV-Borne Spectrometer for Land Cover Classification. *Drones* **2018**, *2*, 16. [CrossRef]
3. Chen, J.; Wang, J.; Wang, W. Robust Adaptive Control for Nonlinear Aircraft System with Uncertainties. *Appl. Sci.* **2020**, *10*, 4270. [CrossRef]
4. Asadi, D.; Ahmadi, K. Nonlinear robust adaptive control of an airplane with structural damage. *Proc. Inst. Mech. Eng. Part G J. Aerosp. Eng.* **2020**, *14*, 2076–2088. [CrossRef]
5. Akhloufi, M.A.; Arola, S.; Bonnet, A. Drones Chasing Drones: Reinforcement Learning and Deep Search Area Proposal. *Drones* **2019**, *3*, 58. [CrossRef]
6. Silvestrini, S.; Lavagna, M. Deep Learning and Artificial Neural Networks for Spacecraft Dynamics, Navigation and Control. *Drones* **2022**, *6*, 270. [CrossRef]
7. Heim, E.H.; Viken, E.; Brandon, J.M. NASA's Learn-to-Fly Project Overview. In Proceedings of the 2018 Atmospheric Flight Mechanics Conference, Kissimmee, FL, USA, 8–12 January 2018; p. 3307.
8. Riddick, S.E. An overview of NASA's learn-to-fly technology development. In Proceedings of the AIAA SciTech 2020 Forum, San Diego, CA, USA, 3–7 January 2020; p. 0760.
9. Chen, S.; Gao, Z.; Zhu, X.; Du, Y.; Pang, C. Unstable unsteady aerodynamic modeling based on least squares support vector machines with general excitation. *Chin. J. Aeronaut.* **2020**, *33*, 2499–2509. [CrossRef]
10. Weinstein, R.; Hubbard, J.E. Global aerodynamic modeling using automated local model networks in real time. In Proceedings of the AIAA SciTech 2020 Forum, San Diego, CA, USA, 3–7 January 2020; p. 0762.
11. Verma, H.O.; Peyada, N.K. Estimation of aerodynamic parameters near stall using maximum likelihood and extreme learning machine-based methods. *Aeronaut. J.* **2021**, *125*, 489–509. [CrossRef]

12. Saderla, S.; Dhayalan, R.; Singh, K. Longitudinal and lateral aerodynamic characterisation of reflex wing Unmanned Aerial Vehicle from flight tests using Maximum Likelihood, Least Square and Neural Gauss Newton methods. *Aeronaut. J.* **2019**, *123*, 1807–1839. [CrossRef]
13. El Gaouti, Y.; Colin, G.; Thiam, B. Online vehicle aerodynamic drag observer with Kalman filters. *IFAC-PapersOnLine* **2021**, *54*, 51–56. [CrossRef]
14. Zhang, W.; Zhu, J. Online identification of aerodynamics with fast time-varying features using Kalman filter. *IET Control. Theory Appl.* **2021**, *15*, 272–280. [CrossRef]
15. Morelli, E.A. Real-time parameter estimation in the frequency domain. *J. Guid. Control. Dyn.* **2000**, *23*, 812–818. [CrossRef]
16. Morelli, E.A.; Smith, M.S. Real-time dynamic modeling: Data information requirements and flight-test results. *J. Aircr.* **2009**, *46*, 1894–1905. [CrossRef]
17. Morelli, E.A. Flight test maneuvers for efficient aerodynamic modeling. *J. Aircr.* **2012**, *49*, 1857–1867. [CrossRef]
18. Kumar, A.; Ghosh, A.K. ANFIS-Delta method for aerodynamic parameter estimation using flight data. *Proc. Inst. Mech. Eng. Part G J. Aerosp. Eng.* **2019**, *233*, 3016–3032. [CrossRef]
19. Sanwale, J.; Singh, D.J. Aerodynamic Parameters Estimation Using Radial Basis Function Neural Partial Differentiation Method. *Def. Sci. J.* **2018**, *68*, 241–250. [CrossRef]
20. Hu, L.; Zhang, J.; Xiang, Y. Neural networks-based aerodynamic data modeling: A comprehensive review. *IEEE Access* **2020**, *8*, 90805–90823. [CrossRef]
21. Li, K.; Kou, J.; Zhang, W. Deep neural network for unsteady aerodynamic and aeroelastic modeling across multiple Mach numbers. *Nonlinear Dyn.* **2019**, *96*, 2157–2177. [CrossRef]
22. Sun, G.; Wang, S. A review of the artificial neural network surrogate modeling in aerodynamic design. *Proc. Inst. Mech. Eng. Part G J. Aerosp. Eng.* **2019**, *233*, 5863–5872. [CrossRef]
23. Winter, M.; Breitsamter, C. Nonlinear identification via connected neural networks for unsteady aerodynamic analysis. *Aerosp. Sci. Technol.* **2018**, *77*, 802–818. [CrossRef]
24. Li, Y.; Liu, X.; He, Q. L1 Adaptive Structure-Based Nonlinear Dynamic Inversion Control for Aircraft with Center of Gravity Variations. *J. Intell. Robot. Syst.* **2022**, *106*, 1–16. [CrossRef]
25. Li, Y.; Liu, X.; Ming, R. Robust dynamic inversion control of flight control system based on L1 adaptive structure. *Xibei Gongye Daxue Xuebao J. Northwestern Polytech. Univ.* **2021**, *39*, 995–1004. [CrossRef]
26. Zhang, Q.; Chen, F.; Li, Z. Time-delay system compensation and intermittent fault tolerance control based on adaptive sliding mode control. In Proceedings of the 2022 5th International Symposium on Autonomous Systems (ISAS), Hangzhou, China, 8–10 April 2022; pp. 1–6.
27. Ijaz, S.; Chen, F.; Hamayun, M.T. Adaptive integral-sliding-mode control strategy for maneuvering control of F16 aircraft subject to aerodynamic uncertainty. *Appl. Math. Comput.* **2021**, *402*, 126053. [CrossRef]
28. He, Q.; Tan, Y.; Liu, X. Reconfigurable nonlinear dynamic inversion for attitude control of a structurally damaged aircraft. *IEEE Access* **2020**, *8*, 199931–199943. [CrossRef]
29. Qiao, F.; Guo, L.; Shi, J. Morphing Aircraft Flight Control Using Nonlinear Dynamic Inversion. In *Advances in Guidance, Navigation and Control, Proceedings of 2020 International Conference on Guidance, Navigation and Control, ICGNC 2020, Tianjin, China, 23–25 October 2020*; Springer: Singapore, 2020; pp. 1519–1529.
30. Safwat, E.; Zhang, W.; Kassem, M. Robust Nonlinear Flight Controller For Small Unmanned Aircraft Vehicle based on Incremental BackStepping. In Proceedings of the AIAA SciTech 2020 Forum, San Diego, CA, USA, 3–7 January 2020; p. 0854.
31. Etkin, B.; Reid, L.D. *Dynamics of Flight: Stability and Control*; John Wiley & Sons: Hoboken, NJ, USA, 1995.
32. Lyu, Y.; Zhang, W.; Shi, J.; Qu, X.; Chen, H. Design of Control Law of Post Stall Maneuver under Unsteady Aerodynamics Based on Improved Dynamic Inverse Method. *J. Northwestern Polytech. Univ.* **2019**, *37*, 523–531. (In Chinese) [CrossRef]

Disclaimer/Publisher's Note: The statements, opinions and data contained in all publications are solely those of the individual author(s) and contributor(s) and not of MDPI and/or the editor(s). MDPI and/or the editor(s) disclaim responsibility for any injury to people or property resulting from any ideas, methods, instructions or products referred to in the content.